6-1-2016

Molecular Dynamics Study on the Grain Growth in Nanocrystalline Aluminum

Jielong Yin
Santa Clara University

SANTA CLARA UNIVERSITY

Department of Mechanical Engineering

Date: June 1, 2016

I HEREBY RECOMMEND THAT THE THESIS PREPARED UNDER MY SUPERVISOR BY

Jielong Yin

MOLECULAR DYNAMICS STUDY ON THE GRAIN GROWTH IN NANOCRYSTALLINE ALUMINUM

BE ACCEPTED IN PARTIAL FULFILLMENT OF THE REQUIREMENTS FOR THE DEGREE

OF

MASTER OF SCIENCE IN MECHANICAL ENGEERING

Thesis Advisor

Thesis Reader

Chairman of Department

MOLECULAR DYNAMICS STUDY ON THE GRAIN GROWTH IN NANOCRYSTALLINE ALUMINUM

By

Jielong Yin

MASTER THESIS

Submitted in Partial Fulfillment of the Requirements
For the Degree of Master of Science
In Mechanical Engineering
In the School of Engineering at
Santa Clara University, June 1, 2016

Santa Clara, California

CONTENTS

LIST OF TABLE

Table page

LIST OF FIGURES

NOMENCLATURE

a	Acceleration
m	Mass
k_B	Boltzmann's constant
r	Distanceρ
t	time
v	Velocity
CS	Centro Symmetric parameter
D	the grain size diameter
E	Energy
Ep	Potential energy
Ek	Kinetic energy
F	Force
N	The atom number in the system
P	Pressure
R	Distance of the cutoff
$\vec{R}_i$	Vector
T	Temperature
T(t)	target temperature
V	volume,
U	Energy
X,Y,Z,x,y,z	Coordinate axis
γ	Position Vector
ρ	Density
T_m	Melting temperature
ψ, θ, φ	The angle between x, y, z axis

ABSTRACT

In recent years, nano-materials have been a popular direction of research in the field of materials science. Nanocrystalline aluminum has been of particular intrest among the nano-materials. This thesis describes the results of three-dimensional molecular dynamics simulations that have been performed to study grain growth in nanocrystalline FCC aluminum. This project built the models by using the Voronoi geometry method to study the grain growth mechanism, grain boundary structure and the effects of temperature and grain size on the crystal structure and grain growth by Energy Analysis, Radial Distribution Function (RDF) analysis, and investigating changes in Centro symmetric parameters.

The results show that nanocrystalline grains are organized and have low energy, whereas grain boundaries consist of distorted regions. The grain growth is controlled by curvature driven grain boundary migration. By analyzing the effect of the temperature and grain size on grain growth, the rate of grain growth increases with increasing temperature. The grain boundary mobility increases with increasing grain size. Grain boundary mobility refers to how easily grain boundaries move, and the grain growth rate is the product of mobility and a driving force term, the later which is inversely proportional to grain size. When the sizes of grains are approximately equal, the curvature direction of initial grain boundary will determine grain growing or shrinking. Grain boundary migration always occurs toward the center of curvature.

Keywords: Grain growth; Grain size; Molecular-dynamics simulation

CHAPTER 1: INTRODUCTION

Nano-materials are widely used and have been a popular direction of research in the field of materials science. Nano-materials have a series of excellent structural and functional properties when compared with traditional coarse-grained materials. One of the most popular nano-materials is nanocrystalline aluminum because of its application in many areas, such as rocket propellants, explosives, and aluminum solar backplanes [1]. As the grains grow in nanocrystalline materials, many of the special properties of these materials significantly diminish or disappear. Grain growth influences material properties which controls the preparation of nanocrystalline aluminum, therefore studying the grain growth of nanocrystalline aluminum has become more and more important.

The grain structure of a polycrystalline material is one of the key factors in determining the physical and mechanical properties of the material. For many applications, the grain size and distribution must be controlled as the changes of grain structure have a significant impact on the properties of materials [2]. There is limited information on the mechanism of grain growth since experimental analysis is typically limited to examining 2D cross sections of 3D specimens. Therefore, analysis of grain growth by computer simulations is generally considered a promising solution. In numerical simulations of grain growth, numerical methods are used to obtain a grain size distribution function [2]. The results are presented using image simulation techniques based on an array geometric design to show the evolution of grain size through the operating procedures.

The purpose of this research is to use molecular dynamics simulation techniques to analyze the micromechanism of grain growth and the influence of the grain size and distribution on 3D grain growth. The study starts with building FCC structures using Voronoi's algorithm theorem. Euler's rotation matrix is used to assign grain-to-grain misorientations. The resulting grain structures are studied using radius distribution function(RDF) analysis, common neighbor analysis(CNA), nanocrystalline sectioning, and potential energy curve analysis.

CHAPTER 2: BACKGROUND AND OBJECTIVES

2.1 Molecular dynamics (MD)

Molecular Dynamics (MD) is one of the most important computer simulations for physical movement of atoms and molecules. Since 1980s, the molecular dynamics method has developed rapidly in many fields such as materials science, nuclear technology, condensed matter physics, chemical reaction kinetics, and biochemistry. The constraint is that the nuclear motion of the constituent particles obeys the laws of classical mechanics, and most notably Newton's law:

$$F = ma \tag{2.1}$$

Since grain growth occurs by the motion of individual atoms, molecular dynamics is an excellent tool for simulating grain growth.

2.1.1 Introduction

In the area of material study, the atom structure model is the basis of all simulations and methods. With improvements in computing power, the models have become more consistent with experimental results. Advanced theoretical methods combined with supercomputers contribute to an understanding with unprecedented detail and accuracy of material behavior at the atomic-level that leads to the birth of the Computational Materials Science. The idea of "Materials calculation and design" in the 1950s formed as a separate emerging discipline in the 1980s [3].

In recent years, developments in fields such as quantum mechanics, statistical physics, solid-state physics, quantum chemistry, computer science and graphics, have allowed for faster computing which provides a powerful tool for material calculations and designs. New technological applications allow for experimental simulations, construction and design of new materials, and the ability to predict the properties of new materials before preparation [1]. Material calculation and design theory have general applicability and guidance for a variety of materials. Their development will improve materials science from the qualitative description of semi-empirical phase into a more scientific quantitative prediction control [4]. Material calculation, design, and computer have become an important branch of modern materials science [5], which include methods such as Monte Carlo, Lattice Dynamics, and Molecular

Dynamics.

In 1957, Alder and Wainwright [6] first used molecular dynamics to study the state equation of gas and liquid in a hard sphere model. This was the first time macroscopic properties of materials were studied using a molecular dynamics simulation. Many improvements have been made to this method, and much research has been done using molecular dynamics simulation for solids, solid defects, and liquids. However, due to limitations in computer processing speed and memory, early spatial scales and temporal scales of the simulation are very restricted. In the late 1980s, the molecular dynamics simulation technology achieved great improvements with the rapid development of computer technology and the development of a multi-body potential function [7]. Molecular dynamics simulations are not as accurate as the first-principles simulations [8], but the program is simple because it has fewer calculations and can calculate larger atomic systems. This chapter outlines the basic principles of molecular dynamics simulations.

2.1.2 The basic idea and principle of molecular dynamics

In molecular dynamics, the system is studied as an overall composition of a large number of particles. A series of information of each particle is obtained by integrating Newton's equations of motion [9], by solving differential equations of Newton's second law:

$$a_i = \frac{d^2 r_i}{dt^2} = \frac{F_i + f_i}{m_i} \tag{2.2}$$

The m_i, r_i, F_i, and f_i represent the mass of i-th atom, the position vector, the force $F_i = -\nabla U(x_i, y_i, z_i)$ which is dependent on the gradient of potential function U, and any other forces that apply to the atom, respectively. The motion trajectories of the system in the phase space can be obtained by solving the equation of motion. Then statistical averaging methods are used to determine the macroscopic quantities [10]. Figure 2.1 shows the molecular dynamics information input and output block diagram.

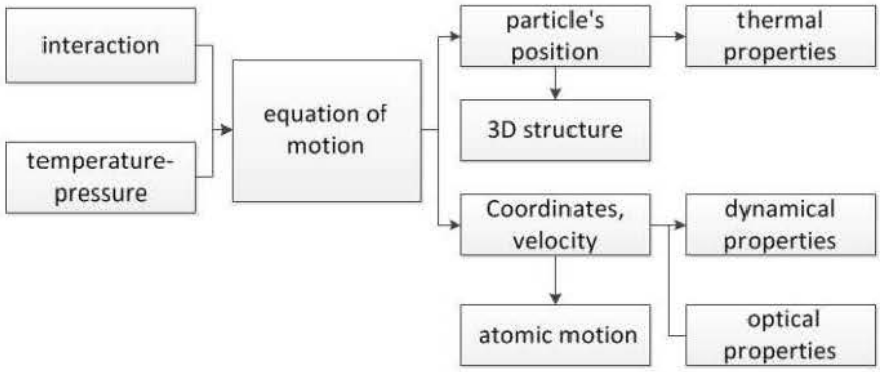

Figure 2. 1 Molecular dynamics information input and output block diagram [10].

2.2 Simulation System

The ensemble consists of a collection of systems which have the same conditions (atom number N, volume V, energy E, pressure P and temperature T) as the studied system [11]. The basic equations are different for each ensemble in molecular dynamics simulation method. Therefore, the MD simulation must be studied in a special ensemble. Depending on the relation between the studied system and a non-controlled external circumstance, the most common ensembles are microcanonical ensembles (NVE), canonical ensembles (NVT), and isothermal isobaric ensembles (NPT).

An NVE is an isolated, conservative and systematic statistic system. In this ensemble, the system phase space evolves along a constant energy trail. In MD simulations, the atoms N, volume V and the energy E of the system will remain unchanged. In an NVT, the system of atoms N, volume V and temperature T remain unchanged. The total kinetic energy is the sum of system energy. Moreover, the total number of all of the atoms in the systems is fixed. In an NPT, the atomic number N of the system, pressure P, and temperature T are unchanged. Temperature is obtained by adjusting the speed of the system or adding a constraint to the system. Adjusting the pressure is complex because the pressure P and the volume V are conjugate variables. The pressure can be adjusted by scaling the system volume.

2.3 Initialization and Boundary Condition

2.3.1 Initialization

In the system, the initial location and initial velocity of all the atoms need to be set before starting the simulation. In the simulation, the initial location depends on the

system structure. In any condition, the location of the atoms cannot contain obvious overlap. In the general case, the location is defined in a box.

Algorithm 1[11]:

```
subroutine init                    //Simulation program initialization
sumv=0
sumv2=0
do i=1,npart
  x(i)=lattice_pos(i)              //fill particle in the lattice
  v(i)=(ranf()-0.5)                //define the random velocity
  sumv=sumv+v(i)                   //velocity center of mass
  sumv2=sumv2+v(i)**2              //kinetic energy
enddo
sumv=sumv/npart                    //systemic velocity
sumv2=sumv2/npart                  //quadratic velocity
fs=squrt(3*temp/sumv2)             //quadratic velocity factor
do i=1,npart                       //set the initial kinetic energy and systemic velocity
are 0
   v(i)=(v(i)-sumv)*fs             // velocity center of mass to zero
   xm(i)=x(i)-v(i)*dt              //atom location previous step
enddo
```

explain:

1) Function (lattice_pos) defines the location of the atom i. ranf( ) defines a uniformly distributed random number. When the systems reach equilibrium, the system's random distribution turns into Maxwell distribution.
2) In a 3D system, the number of degrees of freedom, N_f, is approximated as 3N.

Algorithm1 defines a simple cubic lattice structure system. Firstly, fill the atoms in the lattice and set the velocity value for every atom which is a uniform distribution in the interval [-0.5, 0.5]. It then shifts all velocity to make the total momentum to be zero and adjusts the velocity of the particles to match the mean kinetic energy. In the

equilibrium system, velocity of atom obeys the following equation:

$$< \mathrm{v}^2 >= 3k_B T/m \tag{2.3}$$

v is the velocity of atom, where k_B is Boltzmann's constant, T is temperature, m is mass of the atom.

Using the following relation temperature at time t can be defined:

$$k_B T(t) = \sum_{i=1}^{N} \frac{m\mathrm{v}_i^2(t)}{N_f} \tag{2.4}$$

Equation 2.4 shows that the equation can get the target temperature T(t) at the special time t, by adjusting the velocity by a factor of $T(t)/T$. This initial velocity values will change with the equilibrium state of the system.

It does not use velocity to solve the Newton's Equation. It uses the location of the current moment x and the previous location x_m combined with a computing method of particle force f to compute the location of the next moment. In the beginning of the simulation, it needs to compute the previous location with the preset values. The equation 2.5 can be used to approximatively calculate the previous location.

$$x_m(i) = x(i) - \gamma(i)dt \tag{2.5}$$

2.3.2 Boundary Condition

The molecular dynamic simulation is limited by the computer's performance. According to a recent report [12], a computer is only capable of simulating 10^8 atoms simultaneously, which is significantly less than the number of atoms or molecules in reality. Due to the limited capabilities of computers, Periodic Boundary Conditions is the most efficient and applicable method of simulating the atoms [13].

Periodic boundary conditions are used to simulate a small number of atom systems to study the macroscopic properties. Periodic boundary conditions can be divided into one, two, and three-dimensional systems. Figure 2.2 shows an example of a Periodic boundary conditions system in 2D. Each single cell has eight neighbors in two-dimensional space and 26 for three-dimensional space. Some of the atoms can be out of the two-dimensional cell meaning they come into the cell from a negative direction. Therefore, the number of atoms in one cell is constant [14]. The present simulation will be for pure aluminum, so adsorption is not a possibility, and periodic

boundary conditions should be suitable.

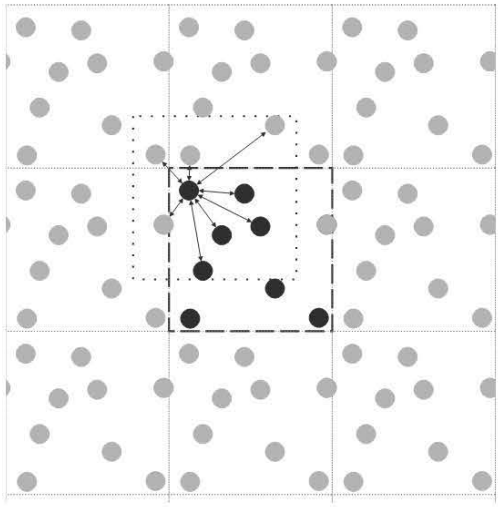

Figure 2. 2 Periodic boundary conditions system [13]

2.4 FCC structure EAM potential

In 1984, Daw and Baskes [15] proposed the Embedded Atom Method (EAM) which is based on the Density Functional Approximation (DFA) theory to overcome the complexities of potential atomic theory and quasi-atomic theory. The basic idea of EAM is that each atom is seen as an impurity embedded in the lattice of other atoms. The energy of each atom is represented as embedding energy and potential energy that are determined by atomic location. The embedding energy can be defined as the difference between the energy of an atom in a homogeneous electron gas and the energy of atom away from the electron gas. The energy expression is:

$$E_{tot} = \sum_{i=1}^{N} E_i \tag{2.6}$$

$$E_i = \frac{1}{2}\sum_j \emptyset_{ij}(r_{ij}) + \mathrm{F}_i(\rho_i) \tag{2.7}$$

$$\rho_i = \sum_j f(r_{ij}) \tag{2.8}$$

where, $\emptyset_{ij}$ is the short-range pair potential; r_{ij} is the distance between atom i and atom j; ρ_i is the density at atom i; F_i is the embedding energy.

Johnson [16] proposed the potential energy of body-centered cubic (BCC) metal based on the EAM. Zhang et.al [20] used this theory to calculate enthalpies of formation for transition metals with BCC structure. The results show the calculated result is different from the experimental results in W-Mo and Ta-W alloy. Depending on his study, Hu et.al [18] added some correct energy terms and improved the

potential function to solve this problem. And they gave more accurate descriptions for potential function expression between metal atoms in different structures. This paper proposed analytic embedded-atom method system which can be used for face-centered cubic (FCC), body-centered cubic (BCC) and hexagonal close-packed (HCP). In this system, the total energy of the atoms can be expressed using the formula below:

$$E_i = \sum_i F_i(\rho_{h,i}) + \frac{1}{2}\sum_{i<j} \varphi_{ij}(r_{ij}) + \sum_i M_i(P_i) \quad (2\text{-}9)$$

$$P_i = \sum_m f^2(r_m) \frac{r_{mx}^2 + r_{my}^2 + \beta r_{mz}^2}{r_m^2} \quad (2\text{-}10)$$

$$\rho_{h,i} = \sum_{i<j} f(r_{ij}) = \sum_{i<j} f_e (\frac{r_1}{r_{ij}})^6 \quad (2\text{-}11)$$

r_m is the distance between i-th atom and its m-th the nearest atom. x, y, z are the components of the three coordinates. The z-axis is parallel to c-axis of HCP crystal, r_{1j} is the distance of first nearest atom (i=1), and f_e is the factor of electron density.

Table 1 summarized the EAM potential parameters and experiment parameters. According to the table, the simulation data is very close to the experiment results.

Table 1: EAM potential and experiment parameters For Aluminum [19]

Lattice properties	Experiment	EAM
a_0 (Å) (300 K)	4.05	4.050
E_0 (eV/atom)	-3.36	-3.360
c_{11} (10^{11} Pa)	1.14	1.13
c_{12} (10^{11} Pa)	0.619	0.616
c_{44} (10^{11} Pa)	0.316	0.320
B (10^{11} Pa)	0.76	0.77
Young's modulus[111] (GPa)	70	69
Shear modulus (GPa)	26	28
Poisson's ratio	0.35	0.36
Phonon frequencies (a_0= *4.030* Å)		
$v_L(X)$ (THz)	9.69	9.62
$v_T(X)$ (THz)	5.80	5.80
$v_L(L)$ (THz)	9.69	9.73
$v_T(L)$ (THz)	4.19	4.17
$v_L(K)$ (THz)	7.59	7.68
$v_{T1}(K)$ (THz)	5.64	5.55
$v_{T2}(K)$ (THz)	8.65	8.63
Vacancy:		
E_f (eV)	0.68	0.67
E_m (eV)	0.65	0.65
Self-interstitials:		
E_f([111]-dumbbell) (eV)	2.80	2.78
E_f([110]-dumbbell) (eV)	2.70	2.47
E_f([100]-dumbbell) (eV)	2.28	2.21
Planar defects:		
γ_{SF} (mJ/m^2)	120~144	117
γ_{US} (mJ/m^2)		158
γ_T (mJ/m^2)	75	62
Surfaces:		
γ_s (110) (mJ/m^2)	980	933
γs (100) (mJ/m^2)	980	855
γ_s (111) (mJ/m^2)	980	634
Melting point:	933 K	850 K

2.5 Grain Growth

Grain growth occurs when materials are subjected to a high temperature.

Reduction in the total grain boundary area scales with the reduction of free energy. The disorganized structure of atoms near the grain boundary induces stress and increases the total energy. The greater the grain boundary energy, the higher the unrestricted energy of the system. The reduction of the grain boundaries energy drives the process of grain growth [20]. Classical models of grain growth state that grain size, D, depends on temperature, second-phase precipitates, and separation and transport of impurity atoms to grain boundary cores [21]. As grains are continually growing and shrinking over time, the mean grain size increases. The mean grain diameter is utilized as a measure of the grain size of an alloy. The Ideal Grain Growth Law relates average grain diameter to initial grain size, and time as seen below.

$$D^n - D_0^n = Kt \tag{2-12}$$

D represents the grain size diameter at time t, D_0 is the initial grain size diameter. K is constant, and t defines time. Early theories of grain growth are based upon the proportionality of the growth rate to the interfacial free energy per unit volume, or they are based on the inverse proportionality of the rate of boundary migration to the boundary curvature, which predict a value of 2 for n [22]. Experimentally it has been shown that values of n lie within the range of 2 to 5. The kinetic exponent, n, within an ideal system controlled by diffusion, has a value of 2, meaning that the system has no defects or precipitates. A value of 3 indicates several phenomena such as precipitate phases with diffusion in the produced grains. If a value of 4 is determined, it means there is an effect of the precipitate with diffusion along the grain boundary [23].

2.6 Grain Boundary

Grain boundary analysis has been a major topic in the field of materials science. The structure of the grain boundary is different from the structure of the grain. There are more lattice distortions in grain boundary which give grain boundary a high boundary energy. And there is a trend that grain boundary spontaneously transforms the high energy state of grain boundary to a low energy state of grain boundary. Grain boundary may change the macro-properties of material such as their physical, chemical, and mechanical properties.

The ultimate goal of the studies on grain boundaries is to identify the relation between grain boundary and macroscopic material properties. That will help us control and design boundaries to generate the target-grain boundaries in the material, and use it

as a basis for design and manufacturing of materials. The current research of grain boundary is divided into two basic directions in the following:

1) The arrangement of atoms is observed by using the experimental method. It uses the relative process to control the grain boundary character distribution. The process is called grain boundary engineering.
2) Using computer simulations to calculate the system-related energy and thermal performance of the grain boundary structure, and also compare the simulation results with experimental results.

In recent years, there are some new viewpoints, which are different from classical Nano model. Gleiter [24] proposed the classical nano model for the first time in his classic paper. He presumes that the grain boundaries of nanomaterials are disorderly gas-like or amorphous structure. They also consider that the grain boundary atom distribution doesn't contain long-range order or short-range order distribution. Additionally, Thomas [25] used a high-resolution electron microscope to directly observe a nanocrystalline grain boundary. They find that there are some certain structures in grain boundary which are different from Gleiter's model. Some other studies [26] have shown that the density of the grain boundary region in a nanocrystalline material is 70-90% of the density of grains region in nanocrystalline material. Meanwhile, these findings show the structure and performance of nanocrystalline grain boundary depend on the nanocrystalline grain. And they found the structure of the nano grain is different from that of the traditional polycrystal. With the nano grain size decrease, the lattice distortion degree increases. These architectural features will influence the macro properties of the nano metal material. In summary, the stability is determined by grain boundary and grain size.

For molecular dynamics study, computer simulation focuses on the method of partial grain growth and the growth mechanism. Computational materials science researchers study grain evolution behavior by nanomaterials simulation and have made some important advances. For example, Haslam [27] studied the growth process simulation of nanocrystalline Pd and pointed out that grain growth mechanisms contain grain boundary migration and grain rotation. Haiyi Liang [28] constructed a numerical model of nanocrystalline copper geometrically by Voronoi and then analyzed the radial distribution function, atomic energy, atomic coordination number,

as well as the center symmetry parameters. The results showed grain has a complete FCC structure. However, there are lattice distortions which the degree of the lattice distortion increases with the decrease of grain size. And there is a highly disordered state in nano boundary structure of nanocrystalline materials, but they were not completely random. Compared with conventional materials, the interface volume percentage is relatively large. So the entropy makes more contribution to specific heat in nanomaterials. Therefore the specific heat of nanostructured materials is much higher than conventional materials. Wei [29] studied the molecular dynamics simulation of thermal stability in nanocrystalline vanadium. The average potential energy from the grain boundary, atomic ratio, and radial distribution function are obtained from the variation of the thermal stability temperature of nanocrystalline vanadium. Wei found that critical temperature of stability decreases when the grain size of nanocrystal vanadium is significantly reduced. Chen [30] found that after a short time, the dependence of average grain radius follows $t^{1/2}$ almost perfectly, independent of the number of order parameters.

There are many studies about nanomaterial grain boundary and grain growth by MD simulation. To provide more support for wider applications of nano-aluminum, this article uses the MD method to study the nano-aluminum grain growth at different temperatures and different sizes.

2.7 Analytical Method

After the MD simulations, the most important issue is how to find a way to distinguish and observe the microscopic defects. There are a variety of algorithms to highlight and distinguish the typical micro-defects. Material scientists are using these algorithms to gain valuable visual documentation. These pictures and videos provide a bridge between the disorganized data and visual structure. Visualization algorithms assist in compressing and reducing a large amount of data calculations. Below lists a few ways to analyze the results.

2.7.1 Energy Analysis

The energy analysis is a good way to determine whether a system is defective. In a system, the defective area has a higher energy. The energy analysis method uses the energy difference to identify the different structure. If the energy of an atom is higher

than a set value, it is considered as a defect. Then use software to color the selected parts. The visualization of these parts is used to show the crystal defects. The energy method has been successfully used to identify micro-cracks, dislocations, nanoholes and other similar defects in the system [31]. Figure 2.3 shows the energy distribution of the grain and grain boundary. The energy analysis is suitable for the analysis of defects in the crystal structure. But it is not suitable for too high temperature.

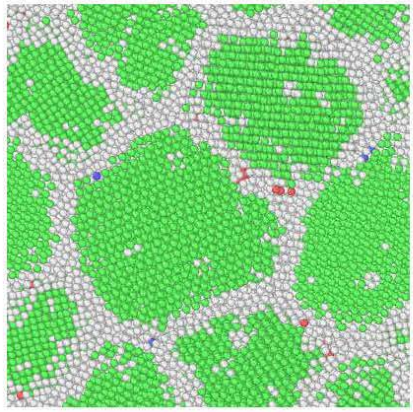

Figure 2. 3 The energy distribution of grain and grain boundary

2.7.2 Radial Distribution Function (RDF)

Radial distribution function g(r) describes how atomic density varies as a function of distance from a reference particle in statistical mechanics [31]. The general algorithm involves determining how many particles are within a distance of r and $r + dr$ away from a particle. When r is small, the distance is short from the target atom, the density of regional atomic is different from the average density of the system. However, when the distance r is far away from the target atom, the densities are same. So the RDF could be close to 1 when r is large enough. Figure 2.4 shows theory of radial distribution function. RDF, $g(r)$, is calculated as follows:

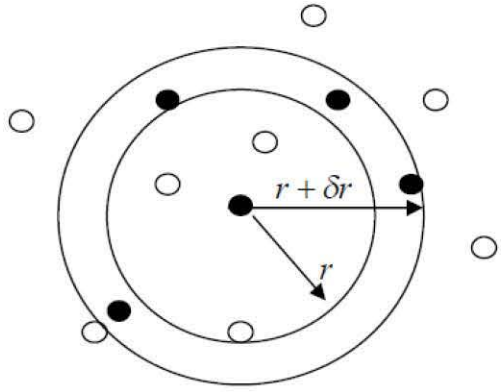

Figure 2. 4 Theory of radial distribution function [31].

$$\rho g(r) 4\pi r^2 dr = dN \tag{3-2}$$

So,

$$g(r) = \frac{dN}{4\pi^2 \rho dr} \tag{3-3}$$

In these equations, N is the atom number in the system, and r is the distance from a reference particle, ρ is the average number density of particles.

2.7.3 Centro-symmetric parameters

Centro-symmetry parameter is used to characterize the degree of inversion symmetry breaking in each atom's local environment. Especially, it is useful for visualizing planar faults in FCC and BCC crystals [32]. For both the centrally symmetric body-centered-cubic and face-centered-cubic materials, the CSP method is useful when studying the internal crystal defects [33]. The study found that each atom of symmetrical center material has a pair of mutually symmetrical reverse atom pairs surrounding it. When homogeneous elastic deformation occurs, the reverse atom of symmetrical relationship does not change and remains intact symmetry. When the material has plastic deformation, the pair of reverse atoms will change the direction or distance between atoms, which will lead to asymmetry. By using centro symmetric materials, the (CSP) can be defined. When the material deforms homogeneously elastically, the parameter is zero. While the material occurs plastic deformation, in cases such as nano indentation, the parameter will not be zero.

The CSP formula is as follows:

$$CS = \sum_{i=1}^{N/2} \left| \vec{R}_i + \vec{R}_{i+N/2} \right|^2 \quad (3\text{-}5)$$

CS is the value of Centro-symmetry parameter. $\vec{R}_i$ and $\vec{R}_{i+N/2}$ are vectors from the central atom to a particular pair of nearest neighbors. When the lattice structure of the material accumulates no damage, $CS = 0$. When there is a symmetrical relation in the reverse atom, $CS = 0$. The symmetrical relationship between reverse atoms can be destroyed because the crystal defects during the plastic deformation, therefore $CS \neq 0$. This varies depending on the type of defect on the crystal. When the crystal has dislocation, twins, and surface or other defects, CS would be different. Based on these CS values, the crystal defects can be differentiated.

2.7.4 Grain Orientation Analysis

Another important analysis method is determining the grain orientation. Firstly, it needs to identify all atoms location in the perfect-crystal local bonding environment. If the atom is located in a perfect crystal environment, there are four nearest neighbors which are situated in the same (001) plane. And the directions of the atoms are along [110] and $[1\bar{1}0]$ directions [34]. The absolute orientation of the grain as a whole is measured using the average orientation, $< \varphi >$, of the four nearest-neighbor vectors of any such perfect-crystal atom. When the grain rotates, its interiors begin to distort slightly. In an attempt to approximate the grains orientation $< \varphi >$ must be determined by averaging the orientations of the atom's bond orientations within a radius of r ($\sim 6a_0$) inside the center of the grain. A lesser value of r must be used for small grains if they are assumed to disappear during the growth process. The value will continue to be used until the disappearing grain is so small that it is no longer viable to assign an orientation. Lastly, by identifying the large clusters of atoms with similar orientations, one can determine the size and shape of the grain.

2.8 Objective

With the continuous development and in-depth research, some new nanomaterials are constantly emerging, and some of the material's unique physical and chemical properties are constantly being recognized and understood. Although research has made significant progress, there are still many problems. Taking into account the limitations of the experiment, this thesis raises awareness to the advantages of

simulation calculations by using molecular dynamics method to study 3D grain growth behavior of aluminum. The purpose of this research is to use numerical simulation techniques to analyze the influence of the grain size and distribution on 3D grain growth to provide insight into the micromechanisms of grain growth. The study starts with building FCC structures using Vornoni algorithm and Euler's rotation theorem to assign grains to the FCC structures. The simulation analysis methods which are used include radial distribution function (RDF), common neighbor analysis method (CNA), nanocrystalline section and potential energy curve.

The main study includes the following:

- Establish Al nanocrystalline system. Build one polycrystalline model using Voronoi method with randomly selected point;
- Analysing grain growth behavior by simulating grain growth at 600K, 675K, 750K, 825K, 900K;
- Use the radial distribution function and the centro-symmetry parameter to study the structure of the grain boundary, the effect of temperature and grain size on the structure of the crystal, the mechanisms of grain growth, and the effect of temperature and grain size on grain growth.

CHAPTER 3: SIMULATION PROCESS

3.1 Building Model

The model building method depends on the Voronoi geometry theory. Assume that there are some random distribution points (3 points in Figure 3.1) in the specific size area. Then using the periodic boundary condition extends the area to a whole plane in 2D which shows in Figure 3.1.

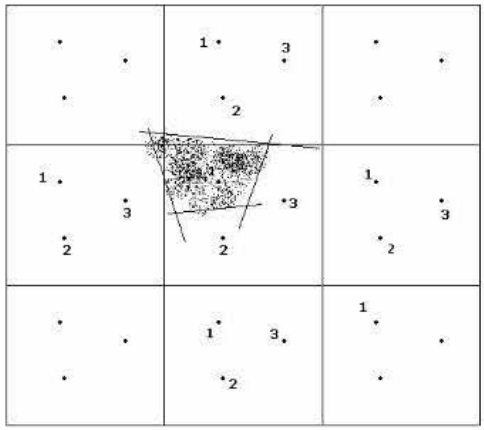

Figure 3. 1 Voronoi plane

The basic approach is:

1. Connect three neighboring points into a triangle and connect all neighboring points by this way [35].

2. Do perpendicular bisector for all triangle's sides.

3. Four perpendicular bisectors create a polygon around one point which showed in Figure 3.1, and more similar polygons can be obtained.

These polygons will be used to build a 2D polycrystalline model. The areas of the polygons are considered as grains, and the boundary of the polygons are considered as grain boundaries.

Depending on this idea, we can build the 3D model.

Firstly, one specific size FCC structure box is built in coordinate system, and some basic coordinate points are randomly picked as datum point in the box.

Secondly, move the whole box from the location of one datum point to origin and move back after random rotation (Eulerian angles). And go through this process from all the datum points.

Finally, it needs to delete the redundant parts outside the box. The rest part is considered as a 3D polycrystalline model.

Atoms are then rearranged, and unsatisfactory atoms are removed. When the distance of two neighbor atoms is less than d_c, one atom is an unsatisfactory atom. The d_c is the nearest neighbor spacing. In the model, the atomic arrangement of different grains is the same except for the grain orientation. The difference of grain orientation is obtained by rotating different angles around the coordinates (Eulerian angles).

Euler angles are a means of representing the spatial orientation of any reference coordinate system as a composition of three elemental rotations starting from a known standard orientation. The reference orientation can be imagined to be an initial orientation from which the frame virtually rotates to reach its actual orientation. In the following, the axes of the original coordination are denoted as x,y,z and the axes of the rotated coordination are denoted as X,Y,Z.

The geometrical definition (sometimes referred as static) of the Euler angles is based on the axis of those mentioned above (original and rotated) reference frames and an additional axis called the line of nodes. The line of nodes (N) is defined as the intersection of the xy and the XY coordinate planes. It is a line passing through the common origin of both frames, and perpendicular to the Z plane, on which both z and Z lie. Figure 3.2 shows the Eulerian rotation [36].

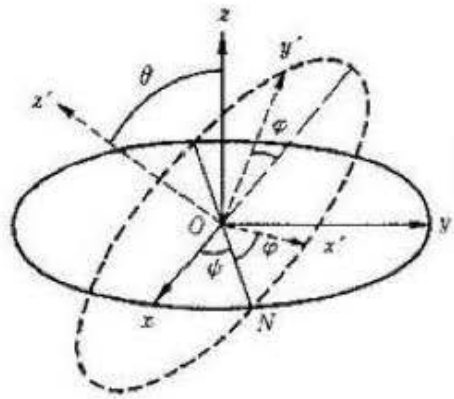

Figure 3. 2 Eulerian Rotation Coordinates [36]

The three Euler angles are defined as follows:

ψ is the angle between the x axis and the N axis.

θ is the angle between the z axis and the Z axis.

φ is the angle between the N axis and the X axis.

If θ is zero, there is no rotation around N. Consequently, Z coincides with z, ψ and φ represent rotations about the same axis (z), and the final orientation can be obtained by a single rotation about z, by an angle equal to ψ+φ.

The final position is calculated by the matrix shown below:

$$R=\begin{pmatrix} \cos\theta\cos\varphi & \cos\theta\sin\varphi & -\sin\theta \\ \sin\psi\sin\theta\cos\varphi-\cos\psi\sin\varphi & \sin\psi\sin\theta\cos\varphi+\cos\psi\sin\varphi & \cos\theta\sin\psi \\ \cos\psi\sin\theta\cos\varphi+\sin\psi\sin\varphi & \cos\psi\sin\theta\cos\varphi-\sin\psi\cos\varphi & \cos\theta\sin\psi \end{pmatrix} \quad (4\text{-}1)$$

θ is called a nutation, φ is called an angle of rotation, ψ is called an angle of precession. This rotation creates different grain orientations.

By the previous method, there are 3 samples that are built. The sizes of the sample are $30a_0\times30a_0\times30a_0$ (Al-30), $40a_0\times40a_0\times40a_0$ (Al-40) and $50a_0\times50a_0\times50a_0$ (Al-50) separately which a_0 is lattice constant of aluminum. There 10 grains in each of the three sample. And there are 51707 atoms in sample Al-30, 103848 in sample Al-40 and 156957 in sample Al-50.

3.2 LAMMPS Process

This thesis presents a methodology for measuring the grain boundary mobility and the activation energy of a curved boundary using a combined atomistic and mesoscopic simulation methodology on microstructure as described in 3.1. To achieve continuous grain growth and minimize the number of different grain boundaries present, this thesis focuses on the model system presented in Figure 3.3.

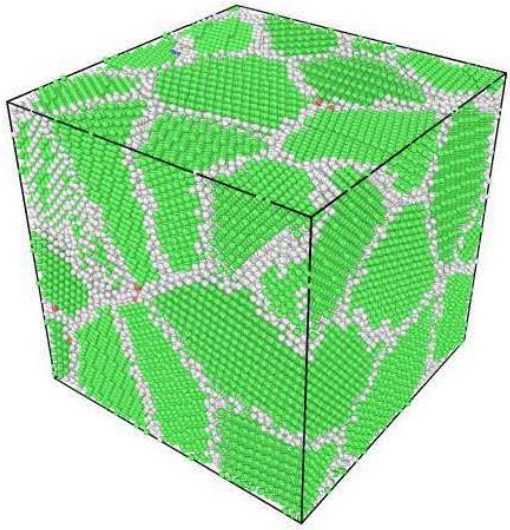

Figure 3. 3 Initial structure of the simulation model

LAMMPS [37] is used to simulate the grain growth process. The three parts of the process are shown in the flowchart presented in Figure 3.4.

1. Read input file;
2. MD simulation;
3. Output.

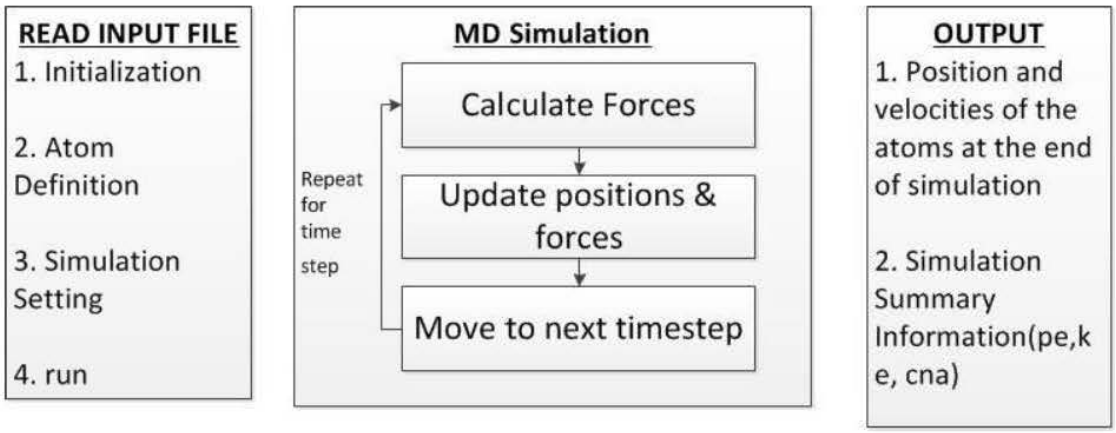

Figure 3. 4 LAMMPS process flow chart

The input file contains initialization, atom definition, and the simulation setting. The initialization is the first stage to set the parameters that define the molecular system and the simulation domain, for example. There are three ways to define the atoms. The details can be read from a new data file, a restart file from the previous simulation, or an input lattice that can be created as part of the simulation itself. Then, the next step is setting the parameters. The location and velocity of each atom will be

determined in the system before running the simulation. In this process, significant overlap cannot occur in the locations of atoms based on the structure of the model. The velocities are dependent on a command that can give each atom a random velocity at temperature 1K. The locations and velocities will be the initial value. Another important setting is a boundary condition. Because the calculated molecules are limited by the speed and capacity of a computer, this research uses periodic boundary conditions to simulate the results. In periodic boundary conditions, the cubical simulation box is replicated throughout space to form an infinite lattice. Simultaneously, the required parameters such as starting temperature, particle number, density, and time to run are set. Once all the required fields are set, the simulation will run for the specified time.

In the simulation process, MD relaxation is conducted in an NPT ensemble environment. The sample was first equilibrated for 50,000 steps with periodicity in all directions which each step is 0.001fs and a temperature of 1K to ensure a stable grain boundary structure. After the initial relaxation, the system temperature increases from 1K to the annealing temperature. The temperature is increased by 1K over 400 time steps. Then the simulation keeps samples at five different annealing temperatures (600K, 675K, 750K, 825K, 900K) for 4,000,000 steps.

CHAPTER 4: RESULT ANALYSIS

In this chapter, the grain growth mechanism in addition to the effect of temperature and grain size on grain growth are analyzed.

4.1 Crystal Structure Analysis

4.1.1 Atom Potential Energy Distribution

Figure 4.1 shows a 2D cross-sectional atomic configuration and Potential Energy Distributions (PED) of the same cross-section. The energy distribution for atoms that are located inside grain region is even. The atomic energy has increased near the grain boundary, suggesting the interior grain structure is more uniform, while the atomic arrange of the grain boundary changes. The potential energy of grain boundary creates a changing crater-shaped distribution. There is no significant difference between the energy of triple junctions and boundaries. This indicates that the degree of disorder and microstructure of the triple grain boundaries are the same as the normal grain boundaries.

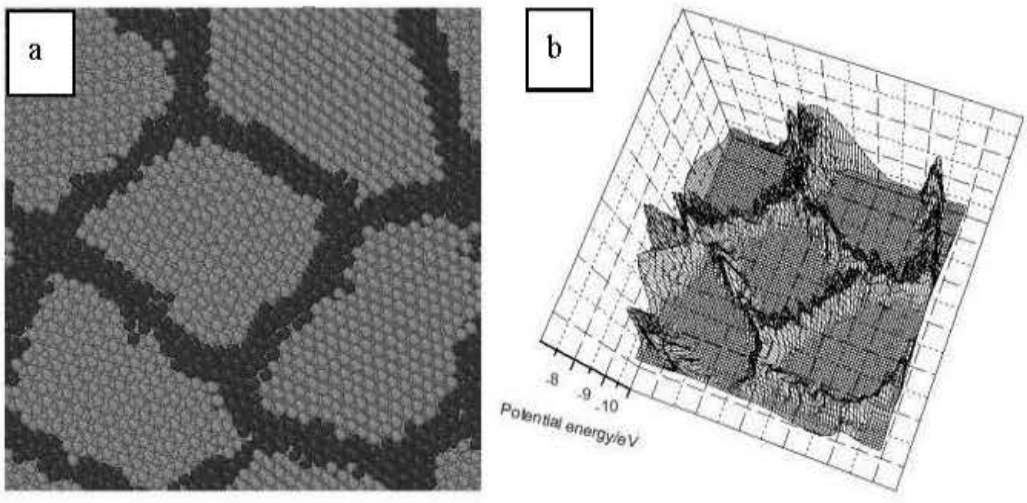

Figure 4. 1 a. 2D cross-section view; b. potential energy distribution of the same area

4.1.2 Effect of Temperature on the energy

The thermal stability of Al is determined by calculating the average energy of the sample atoms as a function of temperature. The energy is calculated mainly by the various pair, bond, etc potentials defined for the simulation by using LAMMPS. Then

the potential energy is calculated as the sum of pair, bond, angle, dihedral, improper, and kspace (long-range) energy [37]. The kinetic energy is calculated by using the equation $E_k = \frac{1}{2}mv^2$. Figure 4.2 shows changes of kinetic and potential energy as a function of temperature. The average kinetic energy and average potential energy show an approximately linear increase with the rise in temperature. The velocity of the atom increases when the temperature rises, causing kinetic energy to increase. This results in heat shock, increase in degree of disorder, and more interatomic potential.

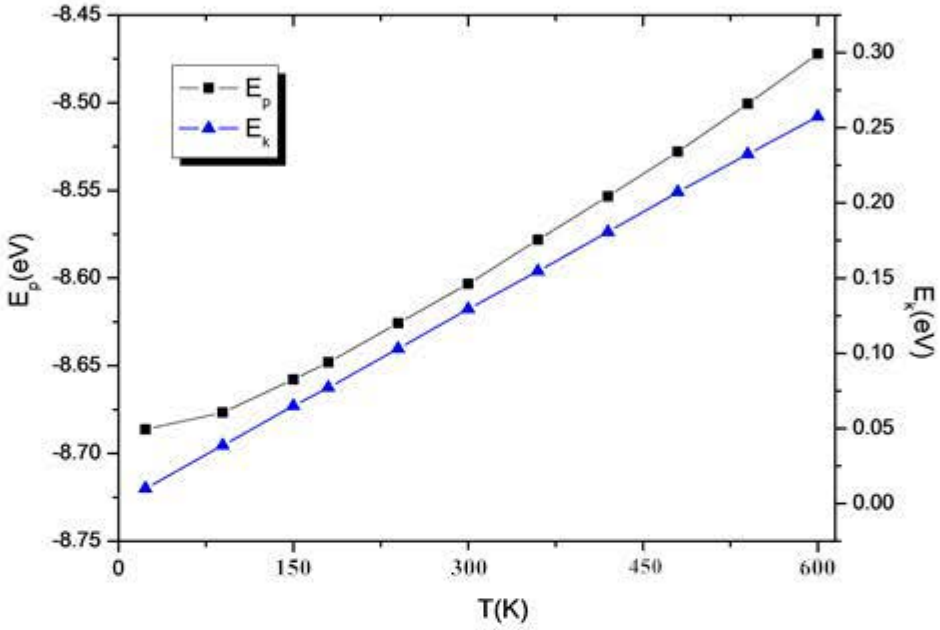

Figure 4. 2 Average kinetic energy and potential energy with the temperature increasing

4.1.3 Effect of grain size on the nano grain structure

This section uses the RDF, as explained in section 2.7.2, to analyze the effect of grain size on the nano grain structure to describe the variation of the structure with the change of the grain size. RDF describes how, on average, the atoms in a system are radially packed around each other. In a perfect crystal, the RDF would consist of infinitesimally narrow spikes at the first nearest neighbor, second nearest neighbor, and all subsequent spacings.

Figure 4.3 shows the radial distribution functions for samples with different grain sizes. R is the distance of the cutoff (the distance setting in LAMMPS, the cutoff is 3.46nm for aluminum). The average grain size is 6.43nm, 8.58nm, 10.73 nm respectively. The value of the spikes increases as the grain size decreased. The reason

is that the rate of the disorder atoms is decreased. The width of the spikes slightly increases as grain size is reduced; however this is not indicative of a fundamental change in the grain boundary structure, but simply results from the fact that a larger fraction of atoms are associated with grain boundaries rather than grain interiors. Further, the locations of the spikes are not obviously changed. That means the structure of grain has not obviously changed. At the same time, it can distinguish the grain atoms and grain boundary atoms by calculating the common neighbor analysis. The above analysis shows that at the grain size studied the material still have crystalline structure.

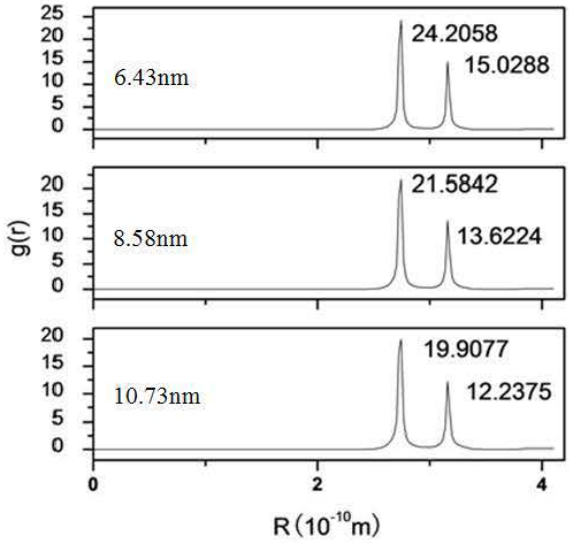

Figure 4. 3 RDF of three simulation system, the average grain size is 6.43nm, 8.58nm, 10.73 nm

4.2 Grain Growth Mechanism

Snapshots for visualization and analysis of the sample were generated to document the grain growth process. Figure 4.4 shows the microstructure development of 3D model after 3ps, at 600 K. The grain and grain boundary defined by different colors.

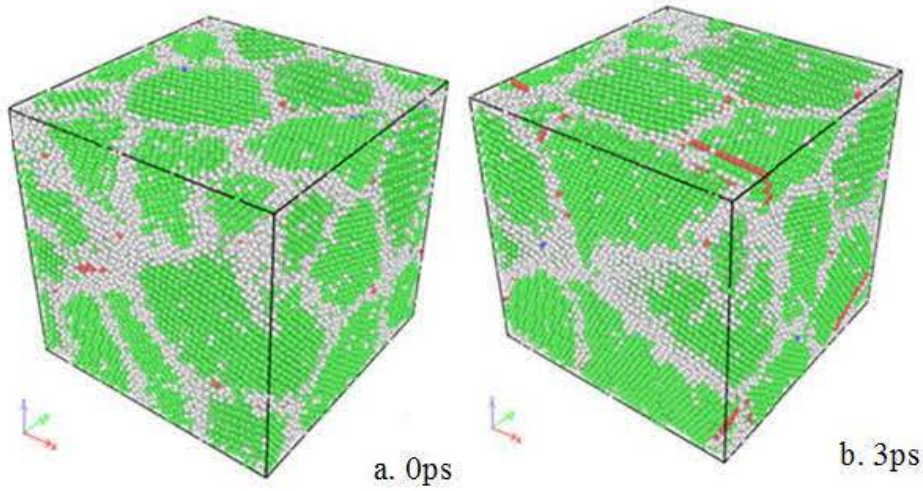

Figure 4. 4 The 3D structure of sample annealing at 600K
a. The structure at 0ps; b. The structure at 3ps

Figure 4.4 shows the initial microstructure with moderately random distributions in the grain's shape. The 3D initial simulation system contains 10 grains, which evolves to a structure comprising of 7 grains in 3ps.

To better represent grain growth, 2D sections of the simulation are shown for grain growth analysis. Figure 4.5 shows a 2D cross-sectional atomic configuration which contains 8 grains at 600K. There are more than 8 grains in the Figure 4.5 which are due to the simulation using a periodic boundary condition. After 3ps all marked grains are present except for grains 4, 5 and 8. The final structure is dominated by grain 3. Analyzing in Grain 3 shows that grain 3 is the largest grain in the initial microstructure. The final microstructure resulted from a series of complex coupled grain boundary migrations and grain coalescence which will be illustrated below.

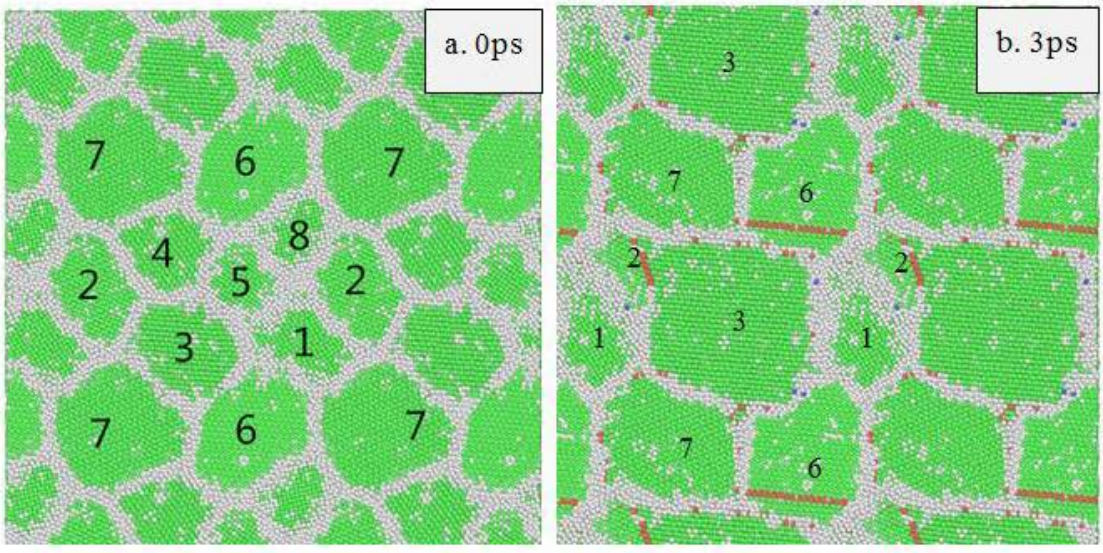

Figure 4. 5 The 2D structure of sample at 600k
a.The structure at 0ps; b. The structure at 3ps

Grain growth is controlled by curvature driven grain rotation and/or boundary migration [34]. To study curvature driven grain rotation, this thesis uses the method which described in section 2.1.4 to determine the orientation of grains. The angles between the grains are calculated which can be used to verify the effect of curvature driven grain rotation. Figure 4.6 shows the chronological progression of the grain's positioning.

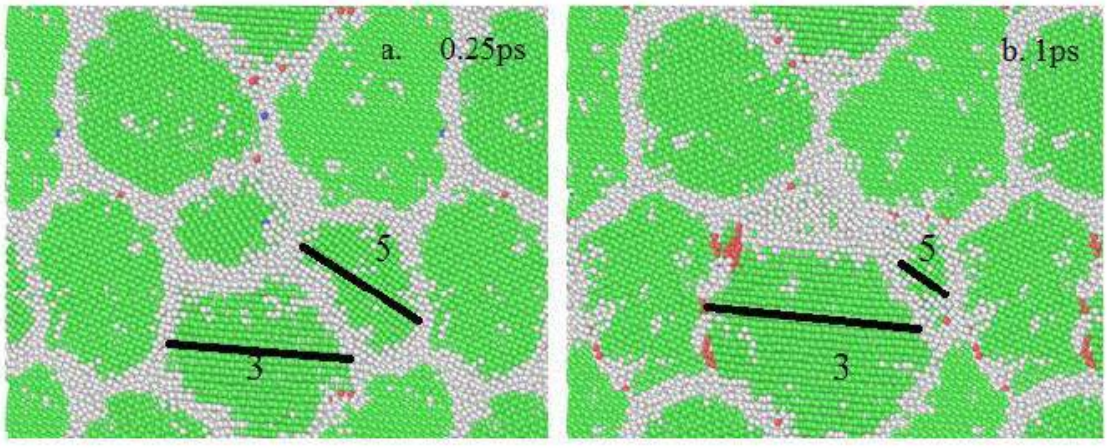

Figure 4. 6 a. the orientation of grain3 and grain5 at 0.25ps, at 600K; b. the orientation of grain3 and grain5 at 1ps, at 600K

From snapshots, we can find that the Grain 3 grows larger while grain 5 shrinks. The curved GB between grain 3 and grain 5 is evident in Figure 4.6, demonstrating GB migration. However, there is no significant change in the angle between the two grains from 0.25ps and 1ps. As shown in Figure 4.7, further analysis of the other angles of

the grains gives the same result. So in this simulation system, curvature driven grain rotation has no obvious effect on the grain growth. The above illustrations demonstrate that GB-migration is the main reason for grain growth in this thesis.

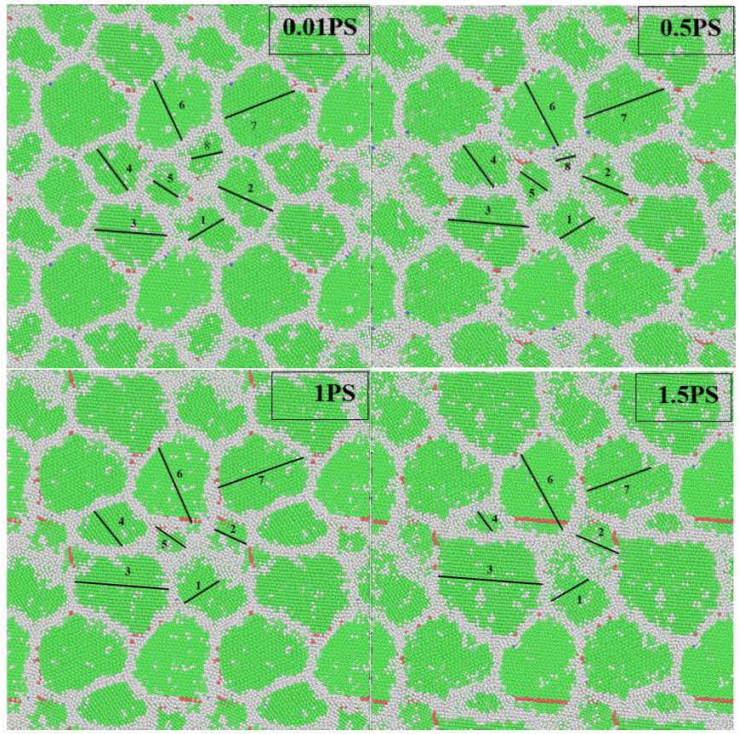

Figure 4. 7 The orientation of grains in this 2D cross-sectional at 600K

For grain boundary migration, the process of the grain growth is shown in Figure 4.8 at 600K. In this figure, 'H' indicates a 'high-angle' grain boundary, while 'L' signifies a 'low-angle' boundary. A 'high-angle' GB is defined by the angle>15° and a 'low-angle' GB is defined by the angle<15°. In order to make the result easier to understand, the grain 8 is chosen as the main object.

By analyzing, we can find that grain 8 shrinks significantly in all of the images above 2ps. The comparison of figure 4.8(a) and (b) shows that the shortening of high-angle GBs happens, and the inclination of the GB between grains 8 and grain 6, 2 changes simultaneously. The lengths of the low-angle GBs between grains 8 and grain 5, 7 remain unchanged. Finally, the high-angle GB between grains 8 and grain 6, 2 has disappeared completely, leaving behind an unstable quadruple junction. Grains 6 and 2 consequently decay into two triple junctions forming a new GB between the two, while grain 8 disappears. This is caused by the high-energy and higher mobility of the high-angle boundary compared to the low-angle boundary. The energy offers the driving force of boundary migration.

Therefore, the high-energy grain boundaries are the main reason for grain growth by curvature-driven GB migration in the system. This is caused by the large amount of energy released by their elimination or change to low-angle GBs, coupled with their high mobility.

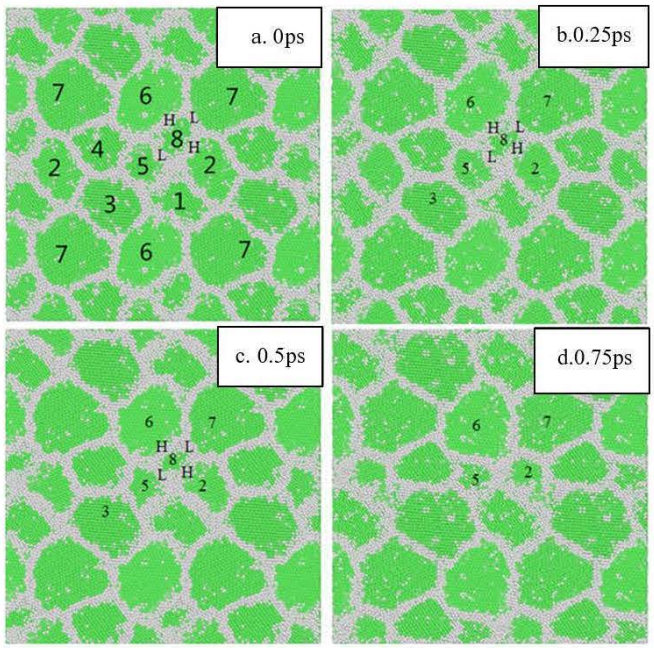

Figure 4. 8 Contraction process of grain 8 at 600K
a. Grains distribution at 0ps; b. Grains distribution at 0.25ps; c. Grains distribution at 0.5ps; d. Grains distribution at 0.75ps

4.3 Effect of temperature on the grain growth

This section analyzes the effect of temperature on the grain growth. After long enough durations of annealing, the result can be used to analyze the influence of the temperature on grain growth. By calculating the number of the FCC atom within each grain, the variation of grain size can be indicated. Analyzing the change of the grain size explains how each grain grows, which offers a better understanding of the grain growth in detail.

Figure 4.9 shows the change of the total number of FCC atom in the system from the simulation done at 600K, 675K, 750K, and 825K. The slopes of the four curves are all positive, meaning during annealing grain growth. However, the different rates of growth are observed for different temperature. A comparison of the four curves shows that the growth rates increases as the temperature rises. Additionally, the increasing rates of the 750K curve and 825K curve have obvious bends. In this simulation, grain boundary mobility is controlled by a single activated process which lammps sets. So

temperature dependence of the boundary mobility may be described by $M = M_0 e^{-Q/k_B T}$, where Q is the activation energy (enthalpy) for migration, k_B is Boltzmann's constant, and M_0 is a (nearly) temperature independent pre-exponential factor [38]. According to the equation, the higher temperature offers more mobility and let special high-angle grain boundary begin to migrate.

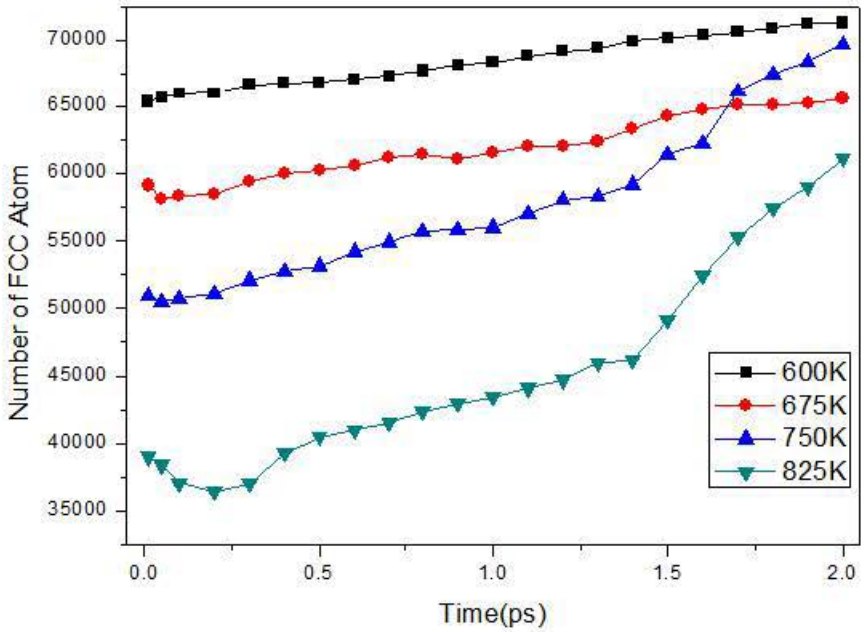

Figure 4. 9 The variation of FCC atoms number at 600K, 675K, 750K, 825K

Figure 4.10 shows the variation in the size of the grain 3. It shows the number of atom in grain 3 increases from 10304 to 19354 at 600K, 8290 to 16952 at 675K, 9925 to 24478 at 750K, and 6496 to 20561 at 825K. The initial numbers of atoms are different because of the different initial temperature. The growth rates appear pretty comparable, but then these seems to be a mechanism change after an initial period in the 750K and 825K data. The mechanism change appears to occur earlier when only grain 3 (one of the more dominant grains) is examined, but nevertheless is reflected in the overall data as well (Figure 4.9). Referencing to the difference of the temperature, the special high-angle grain boundaries do not migrate until they meet the high-temperature requirement.

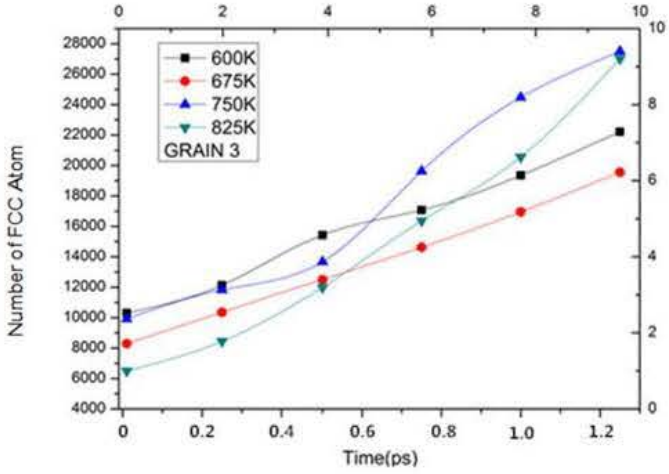

Figure 4. 10 The variation of size of grain 3 at different temperature

The variation of the number of atoms in grain 4 is shown in Figure 4.11. The rising temperatures increase the grain boundary mobility, which promotes grain growth and causes shrinking in small grains. Grain 4 is one of the smallest grains. When the sample is annealed at different temperatures, grain 4 decreases. Moreover, the decreasing rate of grain 4 is slightly increased with the rise of temperature.

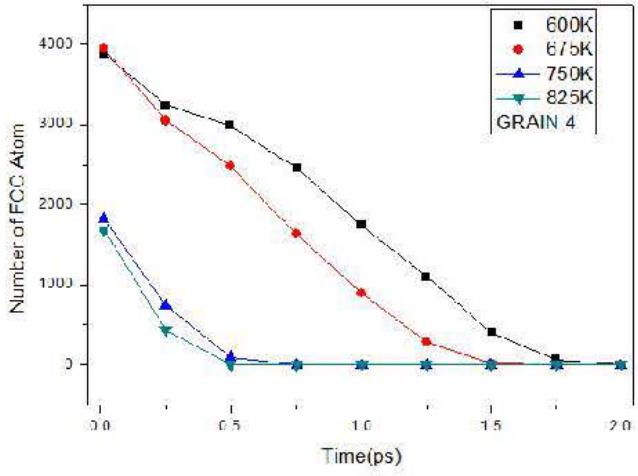

Figure 4. 11 The variation in the number of atoms inside grain 4 atoms number at different temperature

Figure 4.12(a) shows the variation of size for the grain 2. The sizes of grain 2 initially decrease and then remain nearly unchanged with the annealing time at 600K, 675K, and 825K. After annealing, the initial size of grain 2 is small, and the other grain grows by 'eating' grain 2.

However, a different behavior is observed for annealing at 750K. The size of the grain 2 increases at 750K. Figure 4.12(b) show the variation of size of grain 2 and the neighbors of grain 2 at 750K. The illustration indicates grains 1, 4, 5, 7, and 8 are

shrinking, allowing grain 2 to grow. It is because grain 2 initially had a high-energy grain boundary. Some grain boundaries will migrate quickly which cause grain 2 increasing. Moreover, the grain 3 is growing which occupies more new generated FCC atom. Grain 2 and grain 3 increase at 750K

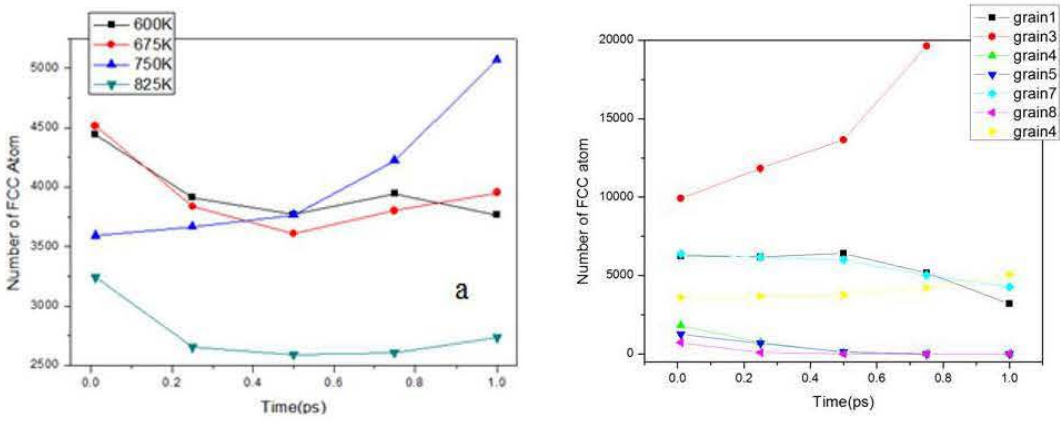

Figure 4. 12 The variation of grain 2 and its neighbors
a. the variation of grain 2 atoms number at different temperatures; b. the variation of the neighbor grains of grain 2 at 750K

The other systems have similar results about the effect of temperature on the grain growth for the variation of the 10 grains. For brevity, the results are not described in detail here. Appendix B shows the variation of the grains in the other two samples.

4.4 Effect of Grain Size on the grain growth

Grain size determines the arrangement of grain boundaries. So grain size will influence grain growth and further influence the property of materials. In this section, by analyzing the variation of grain size, the effect of grain size on grain growth is studied. There are similar results in the three different samples. Here annealing at 600K is analyzed for the A-40 specimen; result for the other two samples are shown in Appendix B.

Figure 4.13 shows the variation of size of all ten grains at 600K. The plots show a significant growth for grain 3, the size of other decrease or remain unchanged. More details are shown in Figure 4.14 and 4.15

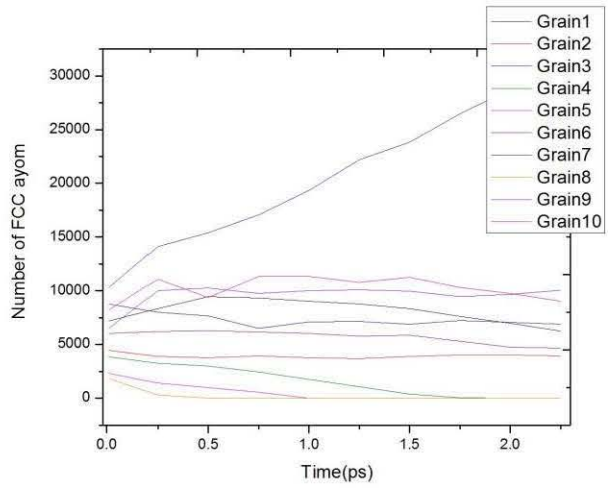

Figure 4. 13 The variation of size of all ten grains at 600K

Figure 4.14 shows the variation of size of grain 3 at 600K. It also shows that grain 3 is the biggest grain in the simulation model, indicating the growth of grain 3 is approximately linear. Grain 3 is the largest, allowing the grain to obtain the long enough curved boundaries. The boundaries have enough energy to drive boundary migration, which drives the grain to continue growing.

As shown in Figure 4.15, the three small grains (grain 4, 5, 8) disappear over time. When other grains grow, the boundaries migration drives these three grains to decrease in size.

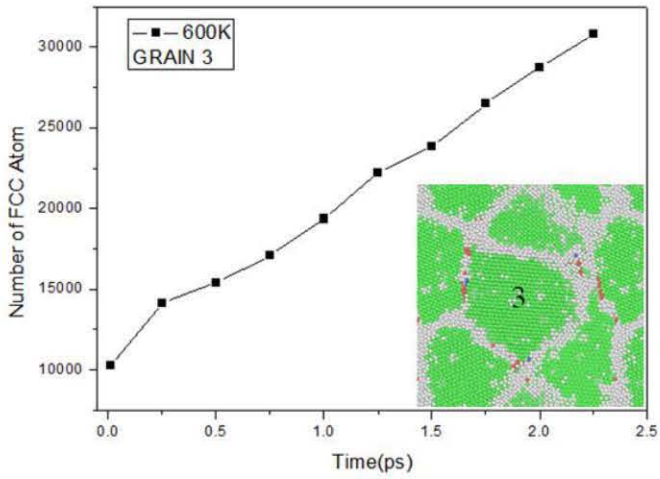

Figure 4. 14 The variation of atoms number of grain 3 at 600K

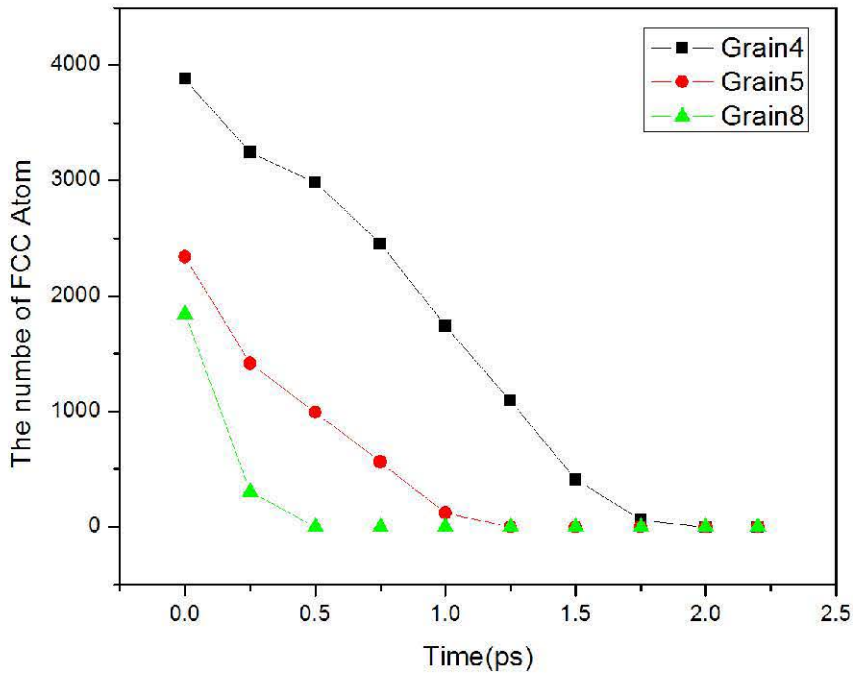

Figure 4. 15 The variation of grain 4, 5, 8 at 600K

Figure 4.16 shows the atom variation of the other six grains. Grains can be divided into two classes:

1) Grains that always remain unchanged. Grain 2, 6, 7 belong to this class. There are low-angle grain boundaries that impede the grains growth.

2) Grains that first grow, and then slightly shrink. In the beginning, these grains grow because the grain has a high-energy boundary. The curvature-driven GB migration makes the grains grow. Then the number of grains decreases which nearly started at 1ps. From the Figure 4.15, the grain 5 and 8 disappear at 1ps. And grain 4 almost disappeared at 1.5ps. That makes the change in the neighboring condition of grain 1, 9 and 10 which lead to the grains shrink. The 2D cross-sectional of the structure is shown in Figure 4.17.

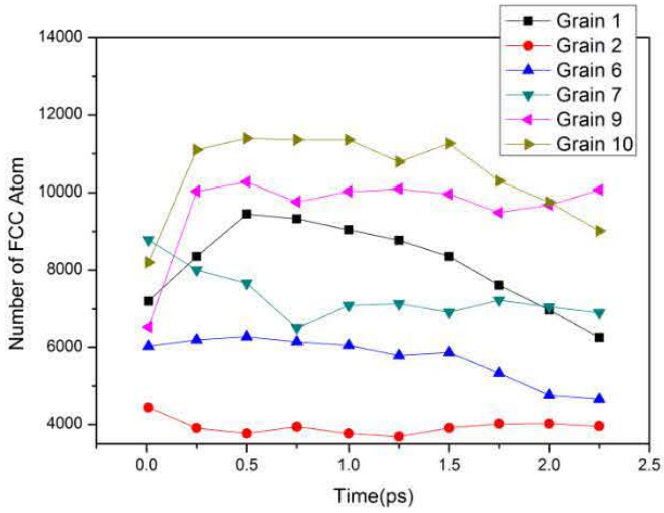

Figure 4. 16 The variation of atoms of grain 1, 2, 6, 7, 9, 10 at 600K

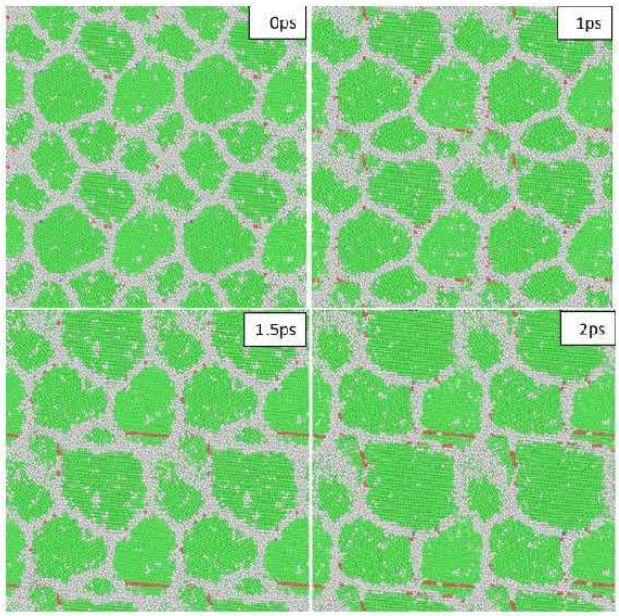

Figure 4. 17 A 2D cross-sectional of the structure at 600K

4.5 Summary and conclusions

This thesis uses the Voronoi geometrical method to build a nano-aluminum polycrystal system. Using the molecular dynamics method, a simulation is performed to study the different model sizes. It analyzes the crystal structure, grain growth mechanism, the effect of temperature, and grain size on the grain growth. The conclusion shows as follow:

1. The initial structure analysis indicates atoms of nanocrystalline grain are high-ordered and have low-energy. The disorganization of the structure is contributed

by the high energy in the grain boundary, and when the temperature rises, the kinetic energy and potential energy increases.

2. It is verified that the grain growth is controlled by curvature-driven boundary migration. Grain rotation minimally affects grain growth in this thesis. Grain growth is dominated by the migration of high-energy grain boundaries in the system which results in a large amount of energy by boundaries elimination.

3. In aluminum simulation system, the rate of grain growth is increased with increasing temperature. When the temperature reaches a special high-value 750K, the grain grows quickly; then it stops growing since there is not enough energy for grain boundary mobility. With continue annealing, the grain boundary gathers enough energy to overcome the resistance. Finally, the neighbors of the grain determine growth direction. From the grain size analysis, the larger sized grains grow, and the smaller sized grains will shrink. Other grains will grow or shrink depend on the neighbors of the grain and curvature direction of initial grain boundary. When the sizes of grains are approximate, the curvature direction of initial grain boundary will determine grain growing or shrinking. Grain boundary migration is always along the direction of the center of curvature. The grain boundary and the neighbors of the grain determine whether the grain grows and the grain direction.

4. The grains are randomly rotated when the model is built. That causes unnecessary structure or vacancy to generate, which directly affects the accuracy of the result. The limitations of the computer's performance have limited the size of the model that can be built. Improving the capabilities of the simulation computer and the model building method would allow for building a bigger size model to get results and analyses that are more accurate.

LIST OF REFERENCES

Electronic Publications:

[1] Zhong, Rong, Hongtao Cong, and Pengxiang Hou. "Fabrication of nano-Al based composites reinforced by single-walled carbon nanotubes." Carbon 41.4 (2003): 848-851.

[2] Frenkel, Daan, and Berend Smit. Understanding molecular simulation: from algorithms to applications. Vol. 1. Academic press, 2001.

[3] Taylor, Charles Fayette. The Internal-combustion Engine in Theory and Practice: Combustion, fuels, materials, design. Vol. 2. MIT press, 1985.

[4] Haile, J. M. Molecular dynamics simulation. Vol. 18. Wiley, New York, 1992.

[5] Monte Carlo and molecular dynamics simulations in polymer science. Vol. 95. New York: Oxford University Press, 1995.

[6] Alder, B. J., and TEf Wainwright. "Phase transition for a hard sphere system." The Journal of chemical physics 27.5 (1957): 1208.

[7] Balbuena, Perla, and Jorge M. Seminario, eds. Molecular dynamics: from classical to quantum methods. Vol. 7. Elsevier, 1999.

[8] Tsuneyuki, S., et al. "First-principles interatomic potential of silica applied to molecular dynamics." Physical Review Letters 61.7 (1988): 869.

[9] Andersen, Hans C. "Molecular dynamics simulations at constant pressure and/or temperature." The Journal of chemical physics 72.4 (1980): 2384-2393.

[10] Zhou. "Molecular dynamic study on intrinsic mechanics behavior of tungsten nanoscale single grystal. " HIT.2012.

[11] Nosé, Shūichi. "A molecular dynamics method for simulations in the canonical ensemble." Molecular physics 52.2 (1984): 255-268.

[12] Nelson, Randolph. Probability, stochastic processes, and queueing theory: the mathematics of computer performance modeling. Springer Science & Business Media, 2013.

[13] Makov, G., and M. C. Payne. "Periodic boundary conditions in ab initio calculations." Physical Review B 51.7 (1995): 4014.

[14] Mosher, Keith, et al. "Molecular simulation of methane adsorption in micro-and mesoporous carbons with applications to coal and gas shale systems." International Journal of Coal Geology 109 (2013): 36-44.

[15] Daw, Murray S., Stephen M. Foiles, and Michael I. Baskes. "The embedded-atom method: a review of theory and applications." Materials Science Reports 9.7 (1993): 251-310.

[16] Ercolessi, Furio, and James B. Adams. "Interatomic potentials from first-principles calculations: the force-matching method." EPL (Europhysics Letters) 26.8 (1994): 583.

[17] Kelchner, Cynthia L., S. J. Plimpton, and J. C. Hamilton. "Dislocation nucleation and defect structure during surface indentation." Physical Review B 58.17 (1998): 11085.

[18] Wangyu HU,BwZhang. Rare Metal Materials and Engineering.1999,28(1):1-4.

[19] H.W. Sheng, M.J. Kramer, A. Cadien, T. Fujita and M.W. Chen, Highly-optimized EAM potentials for 14 fcc metals, PRB 83, 134118 (2011)

[20] Bangwei Zhang, Yifang Ouyang. Analytic EAM potential model for Cr. Chinese Science Bulletin，1993，38：1816.

[21] Abbaschian, Reza, and Robert Reed-Hill. Physical metallurgy principles. Cengage

Learning, 2008.
[22]Yue, Chongxiang, et al. "Kinetic analysis of the austenite grain growth in GCr15 Steel." Journal of materials engineering and performance 19.1 (2010): 112-115.
[23]Singh R, Rajput N N, He X, et al. Molecular dynamics simulations of the ionic liquid [EMIM+][TFMSI−] confined inside rutile (110) slit nanopores. Physical Chemistry Chemical Physics, 2013, 15(38): 16090-16103.
[24]Gleiter, Herbert. Nanocrystalline materials. Springer Berlin Heidelberg, 1991.
[25]Thomas, G. J., R. W. Siegel, and J. A. Eastman. "Grain boundaries in nanophase palladium: high resolution electron microscopy and image simulation." Scripta Metallurgica et Materialia 24.1 (1990): 201-206.
[26]Sui M L, Lu K, Deng W, et al. Positron-lifetime study of polycrystalline Ni-P alloys with ultrafine grains. Physical Review B, 1991, 44(12): 6466.
[27]Haslam, A. J., et al. "Combined atomistic and mesoscale simulation of grain growth in nanocrystalline thin films." Computational materials science 23.1 (2002): 15-32.
[28]Hai Liang,Xiuxi Wang, et al. Nano multi-molecular microscopic structure of crystal copper dynamics simulation. Physics, 2005, 51(10): 2308-2314..
[29]Zhingming Wei, Fang, Yuan, et al. Molecular dynamics study on stability of nanocrystal V. China Science E, 2006, 9.
[30]Chen L Q, Yang W. Computer simulation of the domain dynamics of a quenched system with a large number of nonconserved order parameters: The grain-growth kinetics. Physical Review B, 1994, 50(21): 15752.
[31]Li X, Fei S, Zhang T. Median MSD-based method for face recognition. Neurocomputing, 2009, 72(16): 3930-3934.
[32]Kelchner, Cynthia L., S. J. Plimpton, and J. C. Hamilton. "Dislocation nucleation and defect structure during surface indentation." Physical Review B 58.17 (1998): 11085.
[33]Kelchner, Cynthia L., S. J. Plimpton, and J. C. Hamilton. "Dislocation nucleation and defect structure during surface indentation." Physical Review B 58.17 (1998): 11085.
[34]Haslam, A. J., et al. "Mechanisms of grain growth in nanocrystalline fcc metals by molecular-dynamics simulation." Materials Science and Engineering: A 318.1 (2001): 293-312.
[35]Dirichlet, G. Lejeune. "Über die Reduction der positiven quadratischen Formen mit drei unbestimmten ganzen Zahlen." Journal für die reine und angewandte Mathematik 40 (1850): 209-227.
[36]Slabaugh, Gregory G. "Computing Euler angles from a rotation matrix." Retrieved on August 6.2000 (1999): 39-63.
[37]Plimpton, Steve, Paul Crozier, and Aidan Thompson. "LAMMPS-large-scale atomic/molecular massively parallel simulator." Sandia National Laboratories 18 (2007).
[38]Upmanyu, M., et al. "Misorientation dependence of intrinsic grain boundary mobility: simulation and experiment." Acta materialia 47.14 (1999): 3901-3914.

Appendix

A. The 3D Structure of Al-30 and Al-50

Figure A.1 shows the 3D structure of 10 grain in the sample Al-30.

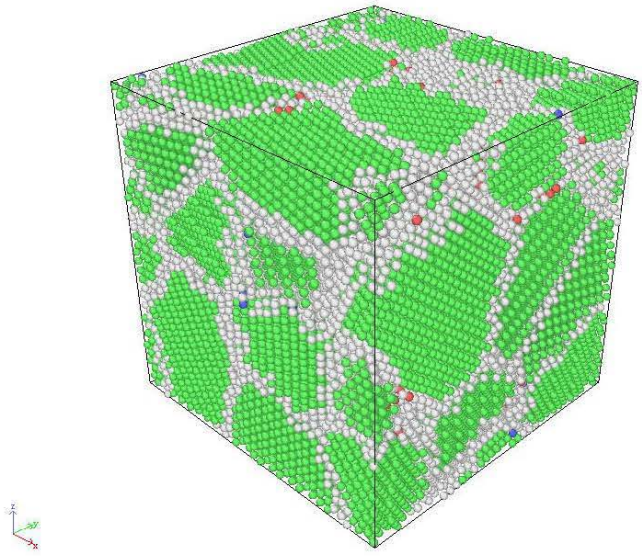

Figure A.1 The 3D structure of 10 grain in sample Al-30

Figure A.1 shows the 3D structure of 10 grain in the sample Al-50.

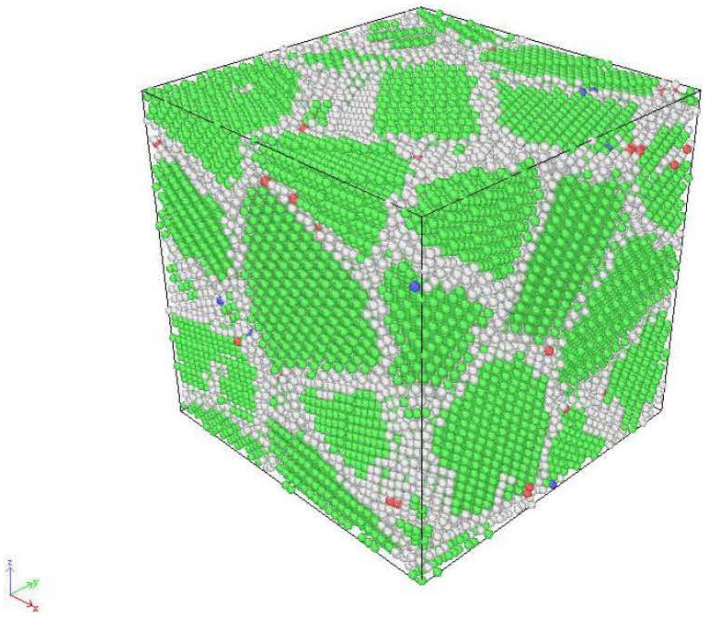

Figure A.2 The 3D structure of 10 grain in sample Al-50

B. The variation of atoms number in sample Al-30 and sample Al-50

Figure B.1 shows the variation of atom number of each grain at 600K in Al-30.

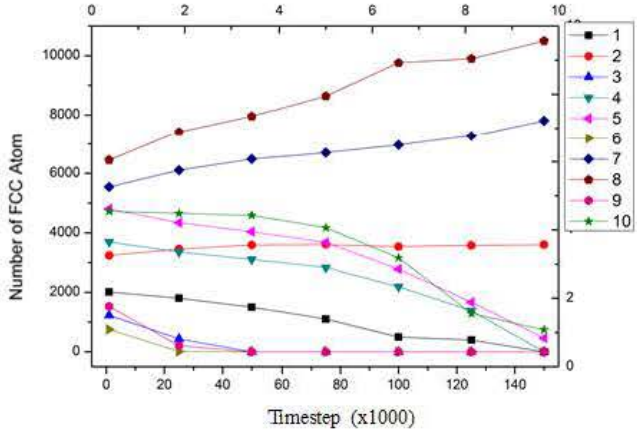

Figure B.1 The variation of atom number of each grain at 600K in Al-30

Figure B.2 shows the variation of FCC atom number at different temperatures in Al-30.

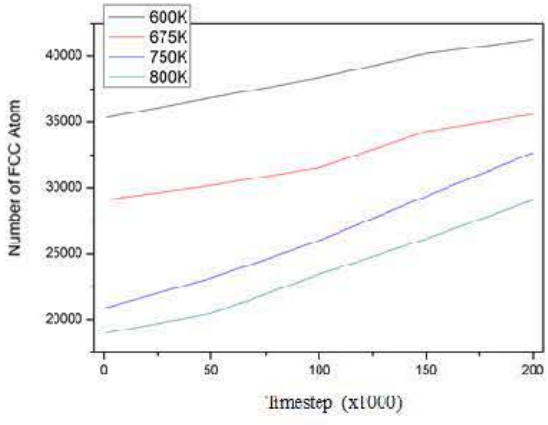

Figure B.2 The variation of FCC atom number at different temperatures in Al-30

Figure B.3 shows the variation of atom number of each grain at 600K in Al-50.

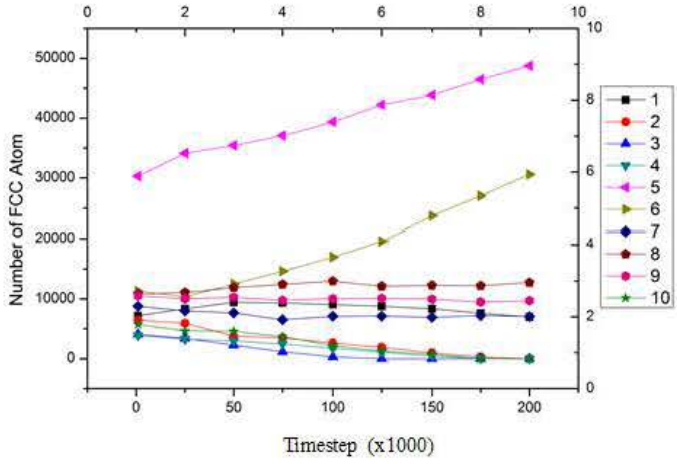

Figure B.3 The variation of atom number of each grain at 600K in Al-50

Figure B.3 shows the variation of FCC atom number at different temperatures in Al-50.

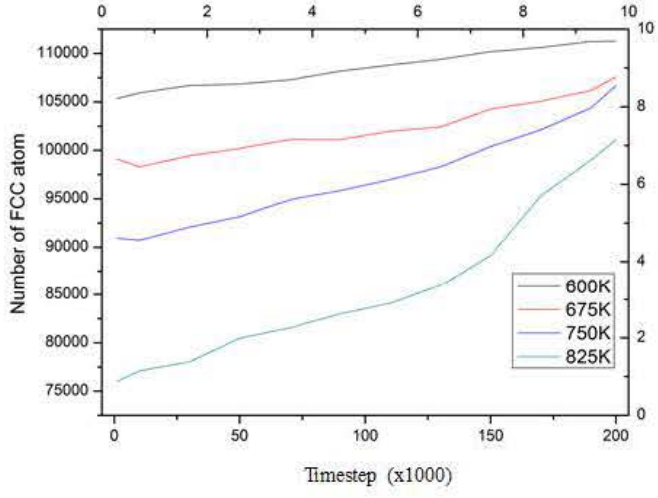

Figure B.4 The variation of FCC atom number at different temperatures in Al-50